SMC Development Guidelines for Axial Flux PM Machines Employing Coreless Rotor Structure for Enhancing Efficiency Based on Experimental Results

Ren Tsunata, Masatsugu Takemoto, Satoshi Ogasawara, Tatsuya Saito, Tomoyuki Ueno

***Abstract*—In recent years, there has been growing demand for flat electrical machines in order to minimize system size while also maintaining high efficiency. In general, axial flux machines (AFMs) are more suitable for flat form than radial flux machines (RFMs). AFMs usually employ a soft magnetic composite (SMC) for the stator core, and their efficiency can be improved by employing an SMC that has low iron loss. However, this reduces the average torque because there is generally a trade-off relationship between iron loss and magnetic permeability in SMCs. The present research therefore proposes an AFM with a coreless rotor structure in which the torque performance is not easily affected by the permeability of the SMC. This research aims to reveal the ideal SMC characteristics for high efficiency in AFMs. First, many virtual SMC materials with different iron loss and permeability are used for simulations of AFMs in order to investigate sensitivity to material properties. The simulations by virtual SMCs take into account the experimental increase in the iron loss. As a result, guidelines for developing SMCs are constructed based on the experimental results. Finally, prototype AFMs employing new SMCs developed by following the guidelines are shown, and it is found that they offer higher efficiency in all operating area than conventional AFMs. In particular, one prototype achieves an extremely high efficiency of over 96% at 6000 rpm, 0.8 Nm in experiments.**

***Index Terms*— Axial flux machine, axial gap motor, soft magnetic composite, coreless rotor, high efficiency, permanent magnet synchronous machine, SPMSM**

I. Introduction

ELECTRIC machines in industrial applications consume over 35%-40% of the electrical energy generated worldwide [1],[2]. This makes it vital to increase the efficiency of electric machines in order to reduce the load on the environment. Permanent magnet synchronous machines (PMSMs) have therefore been used for many applications because of their high efficiency.

On the other hand, there are many applications where flat PMSMs are desired in order to minimize the system size. Currently, most PMSMs can be classified as radial flux machines (RFMs). However, flat RFMs cannot generate enough torque because the air gap area, which contributes to generating torque, is reduced. Therefore, axial flux machines (AFMs) are often used for flat PMSMs [3]-[14]. In recent years, many research groups have conducted investigations into AFMs from the perspective of structure, such as the number of stators and rotors [4],[5] and pole/slot combinations [6],[7]. However, there have been almost no investigations into the characteristics of soft magnetic composites (SMCs) suitable for enhancing the efficiency of AFMs. This paper aims to reveal the ideal characteristics of SMCs for high efficiency in AFMs employing a coreless rotor structure [3],[8] and a wide air gap, as shown in Fig. 1.

Although we previously reported guidelines for developing SMCs for AFMs at ICEM2020 [15], that work did not include experimental results. In other words, the development guidelines were built based purely on simulation results. However, the iron loss of an actual electrical machine is higher owing to the switching ripple caused by the inverter [16], [17]. This paper therefore modifies the development guidelines to take into account experimental results obtained using a prototype with an existing SMC material as shown in Fig. 2. This paper includes experimental results for two prototypes employing newly developed SMCs based on the proposed guidelines. The experimental results and newly developed SMCs support the proposed SMC development guidelines.

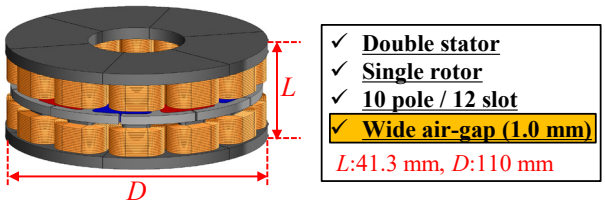

Fig. 1. 3D model of the proposed AFM using a coreless rotor structure.

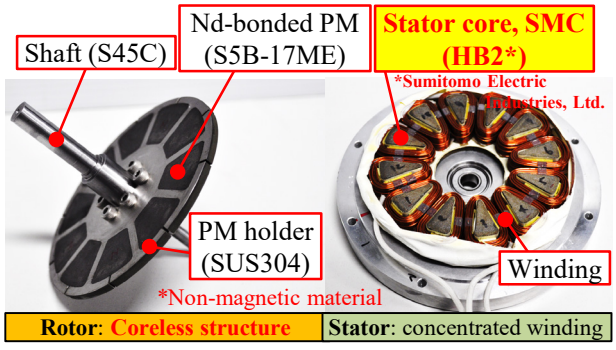

Fig. 2. Appearance of the prototype using existing SMC for the stator core.

This paper is organized as follows. Section II describes the structure and features of the investigated AFM, discusses the effectiveness of the coreless rotor structure, and presents a magnetic equivalent circuit of the AFM. In Section III, simulations are performed of AFMs using many virtual SMC materials with different iron loss and permeability characteristics in order to investigate the sensitivity to material properties. The average torque and the various losses in the AFM are calculated by three-dimensional finite element analysis (3D-FEA). Section IV presents experiments on a prototype using an existing SMC material, and calculates the total loss ratio k based on differences in the total loss between 3D-FEA and the experimental results. The variations in iron loss and efficiency of the AFM are then described over a wide operating area using virtual SMCs considering the total loss ratio k. Based on the results, two SMCs are newly developed in a laboratory (Sumitomo Electric Industries, Ltd.) and adopted for AFMs in Section V. The experimental results clarify the accuracy of predicted efficiency in Section IV. In addition, the effectiveness of the newly developed SMCs is also discussed from the perspective of efficiency. Finally, Section VI illustrates the SMC development guidelines by using some examples, and Section VII concludes the paper. Detailed parameters and the dimensions of the investigated AFM are shown in the Appendix.

II. Characteristics of the Proposed AFM

A. Structural characteristics of the proposed AFM

Figs. 1 and 2 show the 3D model and the prototype of the AFM investigated in this paper, respectively. This structure was previously proposed by our research group [3],[8]. Compared with conventional AFMs, the proposed structure offers the following three advantages:

1) Employs neodymium-bonded permanent magnets (Nd-bonded PMs);
2) Removes magnetic core from the rotor (coreless rotor structure, see Fig. 3(b));
3) Has a wide air gap length of 1.0 mm.

First, the proposed AFM uses Nd-bonded PMs (S5B-17ME, Hitachi Metal, Ltd.) to reduce the eddy current loss in the PMs, particularly at high rotational speeds. AFMs frequently employ neodymium-sintered permanent magnets (Nd-sintered PMs) in order to increase torque density. However, since Nd-sintered PMs have high electric conductivity, large eddy current loss occurs at high rotational speeds. Hence, the proposed AFM can achieve higher efficiency than that of conventional AMFs by using Nd-bonded PMs [18]. In addition, the proposed AFM using Nd-bonded PMs can achieve higher efficiency in high-speed and large-torque region compared with the conventional one employing ferrite PMs because of lower copper loss [18]. Accordingly, the AFM using Nd-bonded PM is a very suitable candidate for industry applications that require continuous operation in high-speed and large-torque region.

Second, the proposed AFM employs a coreless rotor structure as shown in Fig. 3(b). Fig. 3(a) shows a conventional rotor employing a magnetic material (S45C) as the back core. In

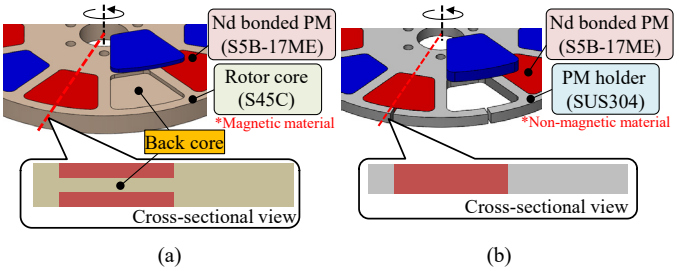

Fig. 3. Rotor structures of conventional and proposed AFMs. (a) Conventional rotor. (b) Proposed coreless rotor.

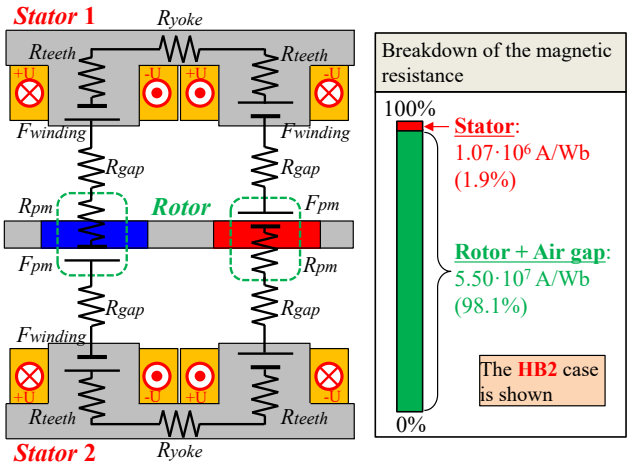

Fig. 4. U-phase magnetic equivalent circuit in the proposed AFM employing a coreless rotor structure and wide air gap.

contrast, the proposed rotor does not have a back core, as shown in Fig. 3(b); we refer to this rotor structure as a coreless rotor structure in this paper. Since the proposed rotor does not need to employ magnetic core in the rotor, a nonmagnetic material (SUS304) is used for the PM holder. The coreless rotor structure offers the following advantages: (i) the thickness of the rotor is reduced by eliminating the back core; (ii) the eddy current generated in the back core is eliminated; and (iii) the thickness of the PMs can be increased, which increases durability against demagnetization while keeping the same volume of PMs [8]. The PMs are fixed on the PM holder by the adhesive, and therefore, it can withstand the electromagnetic force in axial direction. In addition, the proposed rotor has safety factor of 3.95 against the centrifugal force in radial direction at maximum speed under condition without adhesive.

Third, the proposed AFM employs a wide air gap length of 1.0 mm to reduce the need for fine adjustment of the axial rotor position during mass production. Table I shows main geometrical parameters of the proposed AFM. The fractional-slot combination of 10 poles/12 slots is adopted in order to reduce torque ripple [6],[7]. In addition, detailed geometrical parameters is shown in the end of this paper as the appendix.

B. Magnetic circuit configuration of the proposed AFM

Fig. 4 shows a simple equivalent magnetic circuit of the proposed AFM employing a coreless rotor structure and wide air gap length of 1.0 mm. As mentioned earlier, the proposed AFM does not have a magnetic core in the rotor. Therefore, the magnetic resistance of the rotor including the air gap has a very large value. This value is much larger than that of the stator,

with the magnetic resistance in the rotor and air gap accounting for about 98.1% of the total value. In other words, the magnetic resistance of the stator core has a small value of 1.9% in the proposed AFM. It is therefore predicted that the total magnetic resistance of the entire AFM is not strongly affected by the magnetic permeability of SMC materials used for the stator core.

The efficiency can be improved by employing an SMC with low iron loss. However, this decreases the average torque since there is generally a trade-off relationship between iron loss and permeability of SMCs [19]-[21]. On the other hand, the average torque of the proposed AFM is not easily affected by the permeability of the SMC owing to the coreless rotor structure and the wide air gap length. Accordingly, the proposed AFM has the potential to increase the efficiency by employing an SMC with low iron loss without reduction in average torque due to low permeability.

III. 3D-FEA Results Using Virtual SMCs

This section defines and describes virtual SMC materials with different iron loss and permeability. Three-dimensional finite-element-analysis (3D-FEA) results for the case of using the virtual SMCs in the proposed AFM are also included. 3D-FEA model and parameters regarding FEA condition are shown in Table I and Fig. 5, respectively.

A. Existing SMC and virtual SMCs used for 3D-FEA

The characteristics of an SMC are changed by altering the manufacturing method and kind of materials [22],[23]. There is also a trade-off relationship between iron loss and permeability, as mentioned above [19]-[21]. Ref [19] shows the trade-off relationship between iron loss and permeability due to differences in manufacturing methods, and Refs. [20] and [21] discuss the characteristics of SMCs having different mass density and particle size from perspective of iron loss and permeability.

This paper defines many virtual SMCs for 3D-FEA by considering a realistic trade-off relationship between iron loss and permeability based on an existing SMC material. Fig. 6 shows the characteristics of the existing SMC and the virtual SMCs. The existing SMC material is HB2 (Sumitomo Electric Industries, Ltd.), which has relatively low iron loss properties among SMC materials. Fig. 6(a) shows the *B*-*H* curves of the existing and virtual SMCs. The solid line shows the measured *B*-*H* curve of HB2, and the dashed lines show that of the virtual SMCs. The magnetic characteristics of virtual SMCs are obtained by multiplying the magnetic field strength *H* on the horizontal axis by an integer based on the HB2 characteristics. We refer to the magnification of the horizontal axis as the magnetic field strength ratio *Hr* in this paper. *Hr* is defined as

$$Hr = \frac{\mu_{r\_\mathrm{HB2}}}{\mu_{r\_\mathrm{vir}}} \quad (1)$$

where μ_{r_HB2} and μ_{r_vir} are the relative magnetic permeability of HB2 and the virtual SMCs, respectively. For example, for the case of $Hr = 2$, since twice the magnetic field strength is required in order to obtain the same magnetic flux density as HB2, the magnetic permeability of the virtual SMC μ_{r_vir} (= $\mu_{r\_\mathrm{HB2}} / Hr$) is 1/2 that of HB2. Six different virtual SMCs with an *Hr* of 1 to 6 are considered in this paper.

TABLE I. Geometrical and FEM Parameters.

Parameters	Value
Axial length *L* (assembly)	41.3 mm
Outer diameter *D* (assembly)	110 mm
The number of poles / slots	10 poles / 12 slots
The number of nodes (mesh model)	186,314
The number of elements (mesh model)	836,464
Simulation time (1 job)	95 min

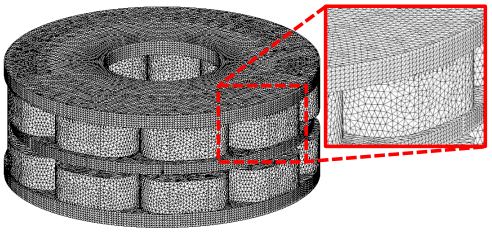

Fig. 5. Mesh model of the proposed AFM.

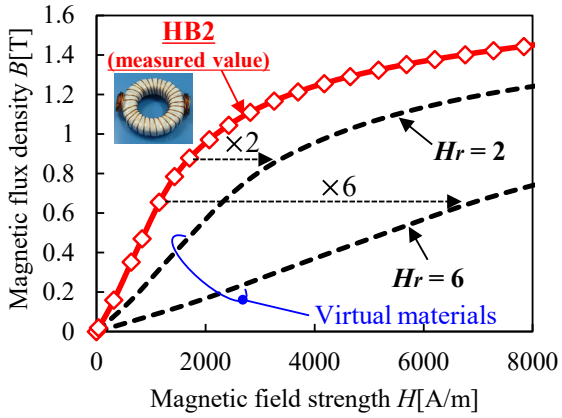

(a)

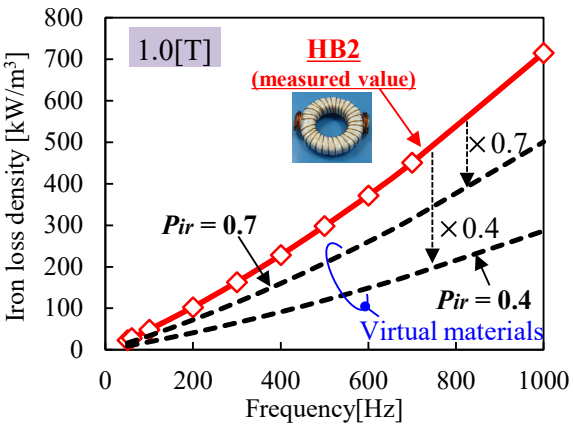

(b)

Fig. 6. Characteristics of an existing SMC (HB2) and virtual SMCs. (a) B-H curves. (b) Iron loss density.

Fig. 6(b) shows the iron losses of the SMCs. The iron loss characteristics of the virtual SMCs as shown by the dashed lines are 0.4 to 1.0 times the iron loss value of HB2, and virtual SMCs having 7 different iron loss characteristics are created considering reality. We refer to the magnification of the iron loss as the iron loss ratio *Pir* in this paper. *Pir* is defined as

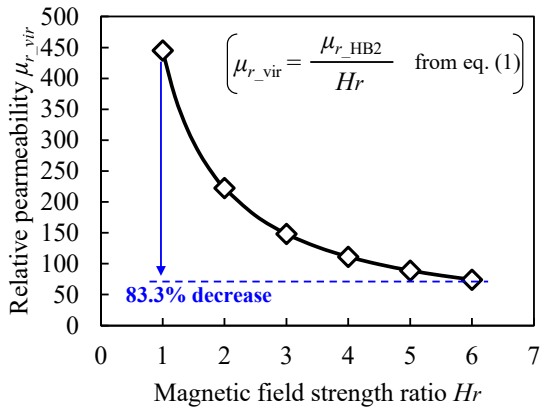

Fig. 7. Change in relative permeability μ_{r_vir} of the virtual SMCs versus Hr.

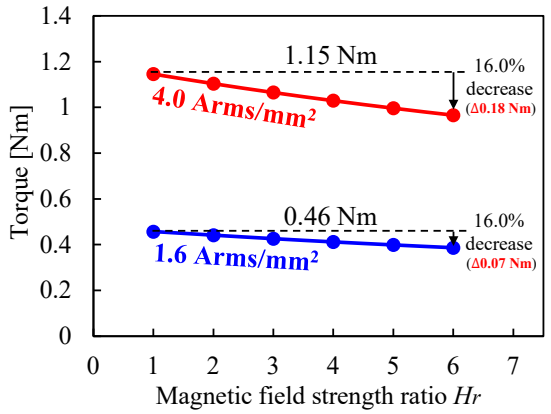

Fig. 8. Change in average torque against Hr under several constant load current conditions (@6000 rpm, Iron loss ratio Pir = 1.0).

$$Pir = \frac{P_{i\_vir}}{P_{i\_HB2}} \quad (2)$$

where P_{i_vir} and P_{i_HB2} are the iron loss of the virtual SMCs and HB2, respectively. From the above, the characteristics of the proposed AFMs employing 41 virtual SMCs and the existing HB2 (Hr = 1, Pir = 1.0) are clarified by 3D-FEA.

B. 3D-FEA results under constant load current

Fig. 7 shows the relative permeability μ_{r_vir} of SMCs versus Hr. The relative permeability is inversely proportional to Hr such that an SMC with Hr = 6 has 83.3% lower permeability than the case of Hr = 1. It is obvious that the permeability of the SMC is strongly affected by Hr.

Fig. 8 shows the change in the average torque versus Hr under constant load current conditions for the case of Pir =1.0 at maximum speed of 6000 rpm. Fig. 8 shows two different current density values for 1.6 and 4.0 Arms/mm^2. The rated current density is set to 4.0 Arms/mm^2 because the proposed AFM can achieve continuous operation without cooling under this condition. Moreover, 1.6 Arms/mm^2 which is less than half of the rated current is chosen in order to evaluate the characteristics in low-torque region. Furthermore, the proposed AFM has the surface permanent magnet (SPM) structure, and hence, q-axis current is only used. Under all current conditions, the average torque decreases as Hr increases because the SMCs with large Hr have low permeability, as shown in Fig. 7. In the

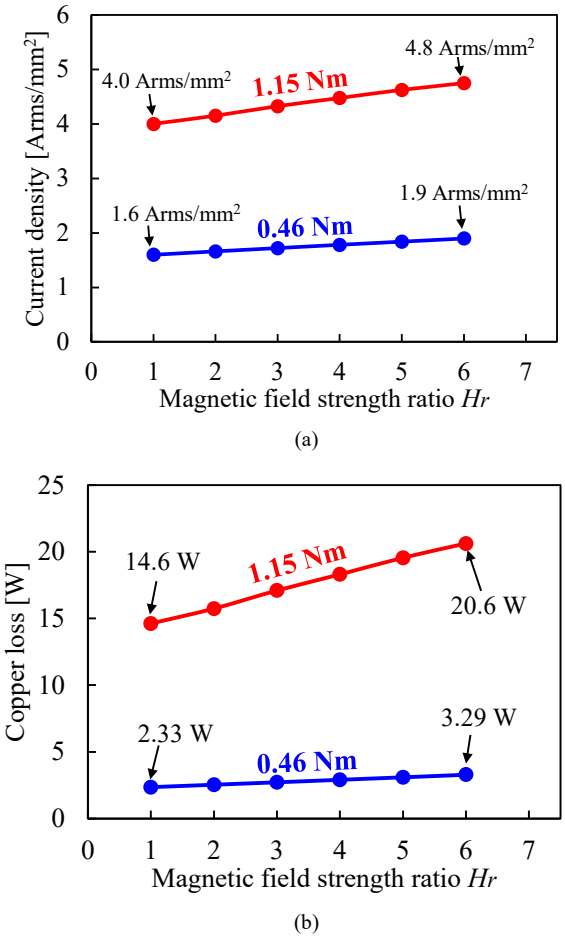

Fig. 9. Current density and copper loss needed to obtain constant average torque in different SMCs. (a) Current density. (b) Copper loss.

4.0 Arms/mm^2 case, the average torque is 1.15 Nm with Hr = 1 (2.93 Nm/L, 1.84 kW/L at 6000 rpm). However, the average torque decreases to 0.97 Nm when Hr is changed from 1 to 6. Although the average torque is reduced correspondingly by 16.0%, the reduction ratio of the average torque is lower than that of the permeability of 83.3%. This is because the magnetic resistance occupied by the SMC in the entire motor is small, and the sensitivity to torque characteristics is low owing to the coreless rotor structure and the wide air gap. From the above results, the coreless rotor structure and the wide air gap are very effective at limiting the reduction in average torque caused by lower permeability SMCs.

In addition, in the case with a current density of 1.6 Arms/mm^2, reduction ratio of the average torque is 16.0%, which is almost the same as the case of 4.0 Arms/mm^2. On the other hand, the net decrease in average torque decreases as the current density decreases when Hr is changed from 1 to 6, as shown in Fig. 8.

C. 3D-FEA results under constant average torque

The average torque needs to be kept constant across all of the virtual SMCs in order to accurately evaluate the iron loss and efficiency under the same operating conditions. In order to keep the output constant, it is necessary to increase the load current to compensate for the decrease in the torque as Hr increases.

Fig. 9 shows the increase in load current density and copper loss when *Hr* is increased while keeping the output power constant at 6000 rpm. The larger the average torque, the higher the increase in current density.

The copper loss also increases with increasing current, as shown in Fig. 9(b). In the proposed AFM, the ac copper loss can be ignored because winding diameter is small (0.4 mm), and therefore, it is not considered in Fig. 9(b). The increase in the copper loss in the case of an average torque of 1.15 Nm in particular is much larger than the case of torque of 0.46 Nm because the increase in current is larger. In summary, the copper loss sensitivity to *Hr* is higher in the region where the torque is large.

Fig. 10 shows magnetic flux density distributions in the stator core using different SMCs having *Hr* = 1, 6. The operating conditions are 6000 rpm and 1.15 Nm, and the load current is varied with *Hr* in order to keep the output power constant. Moreover, the magnetic flux densities along the line from *A*' to *B*' at the top of the tooth where the magnetic flux density is the highest are shown in Fig. 10. The solid line and the dashed line show values under load and no-load conditions, respectively. As *Hr* increases, the magnetic permeability of the SMC decreases, and the magnetic flux density of the stator core slightly decreases. The stator core with *Hr* = 6 has lower magnetic flux density compared with case of *Hr* = 1, although the torque is same. This difference is caused by the increase in magnetic resistance in the AFM. As a result, the iron loss in the stator core can be reduced under the same operating conditions by increasing *Hr*. In other words, if the decrease in iron loss due to low magnetic flux density is greater than the increase in copper loss, the efficiency can be improved by simply lowering the permeability of the SMC. The efficiency under operating area where iron loss is dominant is more likely to be improved.

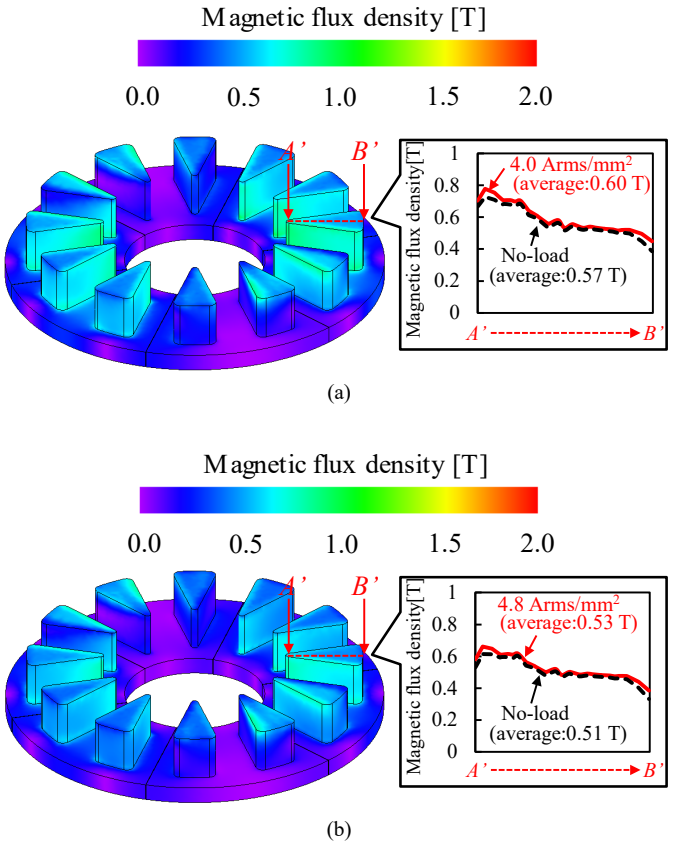

Fig. 10. Magnetic flux density distributions in the stator core of the proposed AFM using different SMCs (@6000 rpm, 1.15 Nm, P_{ir} = 1.0). (a) *Hr* = 1: permeability is same as HB2. (b) *Hr* = 6: permeability is 1/6 of HB2.

IV. Investigation of Efficiency by 3D-FEA with Virtual SMCs Considering Experimental Results

In the previous section, 3D-FEA analysis was performed of an AFM employing virtual SMCs, and the variations in torque, copper loss, and magnetic flux density were discussed. The iron loss of actual machine in experiments is generally higher owing to the switching ripple caused by the inverter [16],[17] and construction factors such as residual stress [24]. Accordingly, it is not desirable to construct SMC development guidelines based on 3D-FEA results alone. Therefore, in this section, experiments are conducted on a prototype using an existing SMC (HB2), and the effect of the experimental increase in the loss is evaluated. These results are then taken into account in the subsequent 3D-FEA and investigations using virtual SMCs.

A. Experiments of the AFM employing existing SMC (HB2)

Fig. 11 shows the test platform and the prototype using HB2 for the stator core. Fig. 12 shows measuring equipment and an inverter used in experiments. The average torque and input power are measured by a torque meter (TH2504, Ono Sokki Co., Ltd) and a power meter (WT1800, Yokogawa Test & Measurement Co., Ltd), respectively. Fig. 13 shows the efficiency maps obtained by 3D-FEA and experiments,

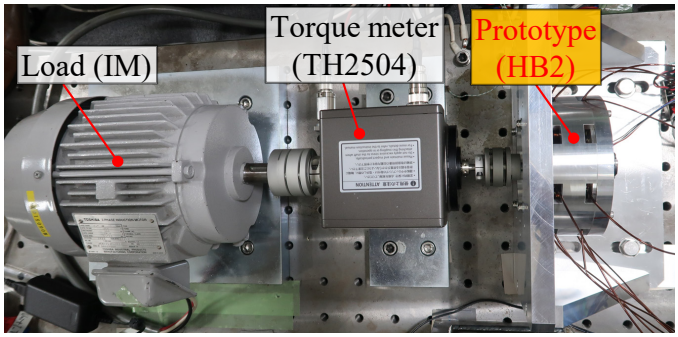

Fig. 11. Appearance of test platform and prototype using existing HB2.

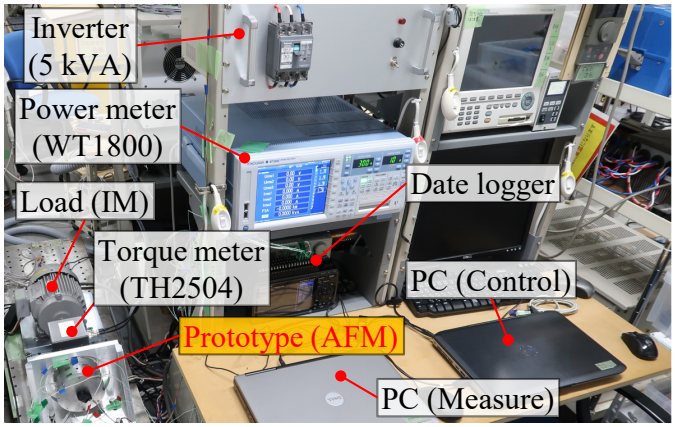

Fig. 12. Measuring equipment and inverter used in experiments.

respectively, in the proposed AFM using HB2. Both results show the same tendencies in terms of efficiency, with the highest efficiency appearing at 6000 rpm, 4.0 Arms/mm^2 in both maps. The proposed AFM achieves a high efficiency of over 90% in the high-speed and large-torque regime because it employs Nd-bonded PMs [18].

However, the efficiency differs between the 3D-FEA and experimental results. It is thought that this difference is caused by the increase in the iron loss in the experiments. Accordingly, in order to take this variation in the efficiency into account when constructing SMC development guidelines, the total loss ratio k map is calculated, as shown in Fig. 14. The total loss ratio k is defined as

$$k = \frac{P_{\text{loss\_EXP}}}{P_{\text{loss\_FEA}}} \tag{3}$$

where $P_{\text{loss\_EXP}}$ and $P_{\text{loss\_FEA}}$ are the total loss obtained by experiments and 3D-FEA, respectively. It is obvious from Fig. 14 that k depends on operating area. The virtual SMCs under all operating conditions are then adjusted by multiplying the total loss obtained by 3D-FEA by the total loss ratio k. This makes it possible to construct SMC development guidelines that take experimental results into account.

This paper defines 6 operating conditions (from *Point-A* to *Point-F*) as shown in Fig. 14. The maximum rotational speed is set to 6000 rpm because many PMSMs in industrial applications such as water pumps have almost the same value [25]. In addition, operating points at 1.15 Nm and 0.46 Nm are defined as heavy load and light load, respectively.

B. Loss and loss ratio at 6 operating points in different SMCs

All remaining 3D-FEA results are adjusted by the total loss ratio k obtained by the experiments on the prototype. Fig. 15 shows iron loss maps at the 6 operating points when all 42 SMC materials are applied to the proposed AFM. In all maps, the vertical axis is the iron loss ratio Pir and the horizontal axis is the magnetic field strength ratio Hr. Based on an existing SMC (HB2) with Hr and Pir of 1, the iron loss of the proposed AFM becomes smaller as Pir becomes smaller under all operating points since the iron loss of the SMC decreases.

Furthermore, it is obvious that the iron loss can be reduced by increasing Hr compared with HB2 even if Pir is not changed. One of the reasons is that the magnetic flux density in the stator core decreases as Hr increases, as shown in Fig. 10. The same tendency is observed under all operating points.

At 1.15 Nm operating *Points-A*, *-B*, and *-C*, the iron loss decreases as the rotational speed increases regardless of Hr and Pir. Moreover, as Pir decreases, the decrease in the iron loss at *Point-C* becomes larger than that at *Point-A* because the iron loss is dominant at *Point-C*.

Fig. 16 shows loss ratio σ maps at 6 operating points. The loss ratio σ is defined as

$$\sigma = \frac{P_c}{P_i} \tag{4}$$

where P_c and P_i are the copper loss and iron loss, respectively. Although the loss ratio exhibits virtually the same trend at all

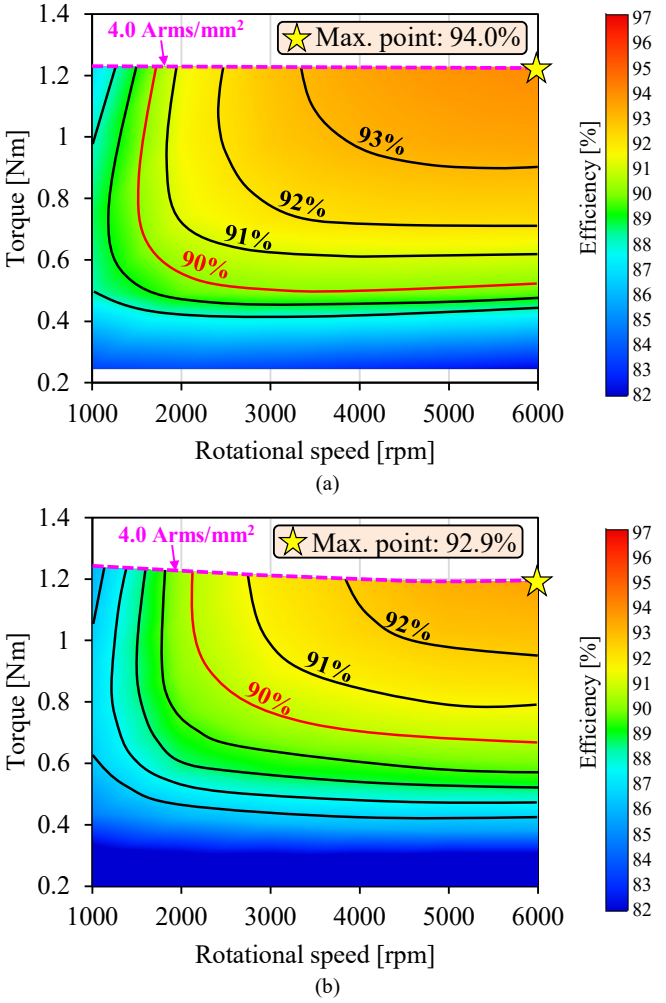

Fig. 13. Efficiency maps of the proposed AFM employing existing HB2. (a) 3D-FEA results. (b) Measured results in experiments.

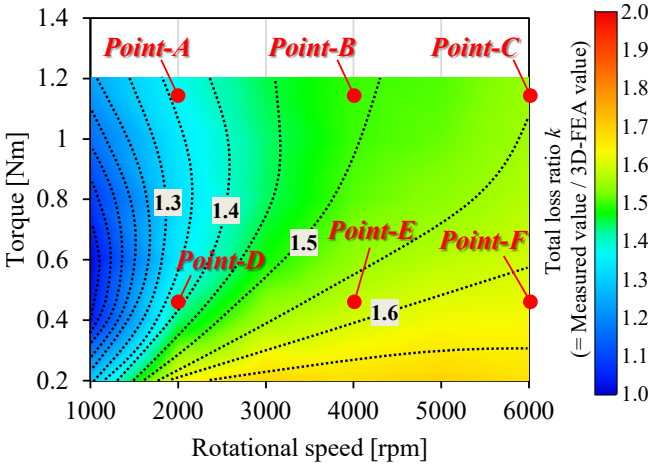

Fig. 14. Total loss ratio k map comparing measured values with 3D-FEA (Total loss ratio k = measured value / 3D-FEA value).

operating points, the sensitivity to Hr and Pir differs. At *Point-A*, the loss ratio σ is higher than at the other operating points because the copper loss is dominant owing to the low-speed of 2000 rpm and heavy load of 1.15 Nm. This means that reduced iron loss does not have a very large impact on efficiency at *Point-A*. In contrast, at *Point-F*, the loss ratio σ is lower than 0.5

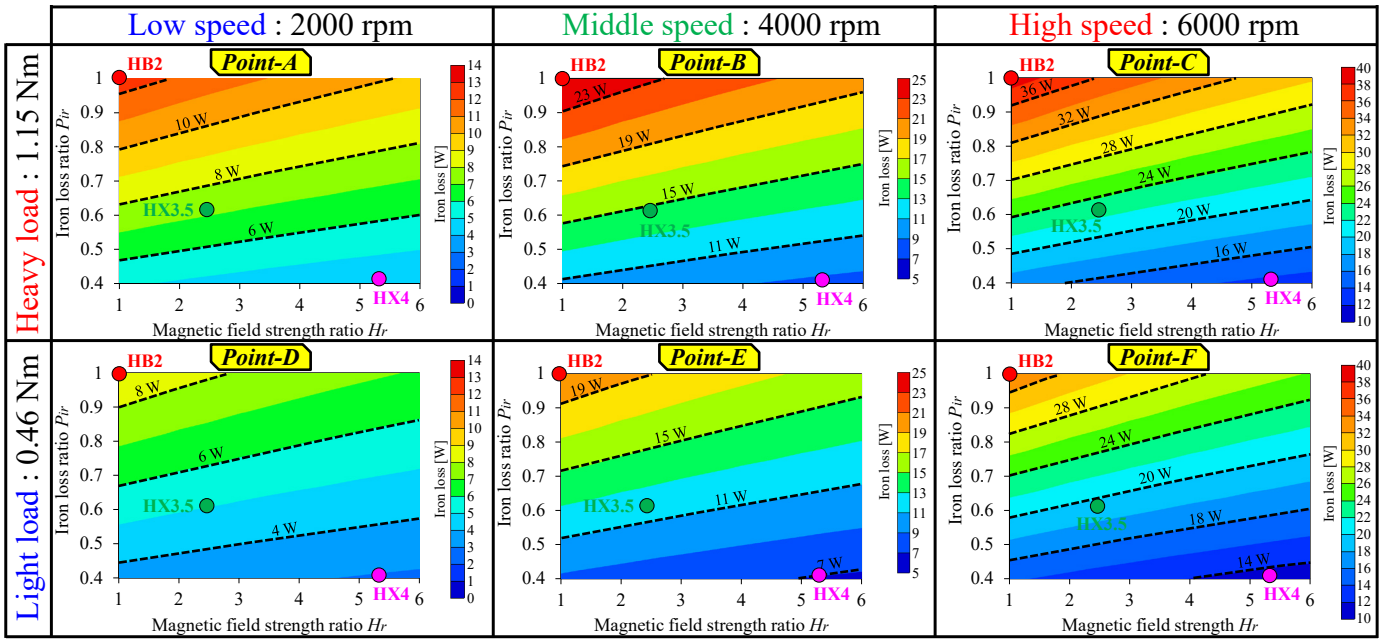

Fig. 15. Iron loss maps at some operating points under constant average torque condition in different SMC materials (Hr = from 1 to 6, Pir = from 1.0 to 0.4).

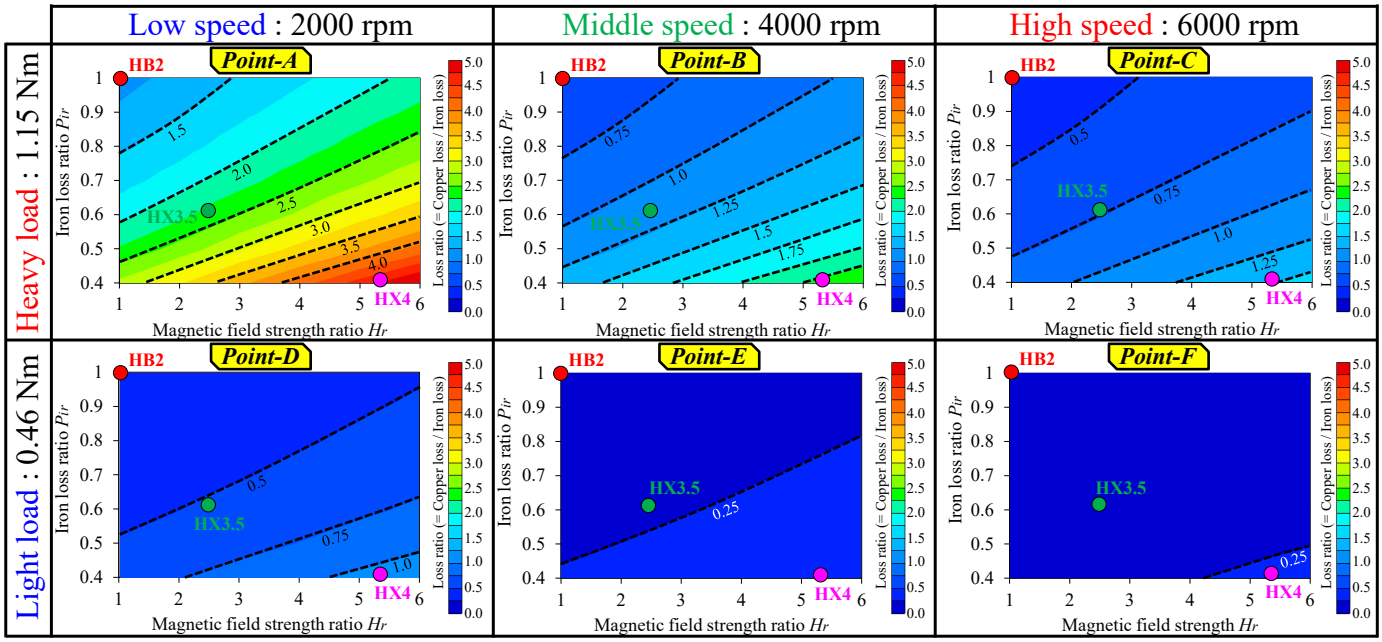

Fig. 16. Loss ratio σ (= Copper loss / Iron loss) maps at some operating points under constant average torque condition in different SMC materials (Hr = from 1 to 6, Pir = from 1.0 to 0.4).

in all SMCs because the iron loss is dominant at this point. Therefore, the impact on the efficiency of decreasing the iron loss is large. From the above, in the efficiency maps against Hr and Pir, it can be predicted that sensitivity to Hr and Pir strongly depends on the operating point of the AFM.

C. *Efficiency at 6 operating points in different SMCs*

Fig. 17 shows efficiency maps at the same 6 operating points as in Figs. 15 and 16. The efficiency in Fig. 17 is calculated by considering the total loss ratio k, as discussed above. In addition, the characteristics of the newly developed SMC materials (HX3.5, HX4) in this research are also plotted on the efficiency maps. These new SMCs are described in detail in Section V. Efficiency maps at all operating points have markedly different tendencies in terms of efficiency because there is a large difference in the loss ratio σ depending on the operating conditions.

First, at *Point-A*, the iron loss is very small because of the low rotational speed. Accordingly, the iron loss is not dominant in the total loss at *Point-A*, as shown in Fig. 16. Thus, reducing the iron loss of the SMC is not very effective for increasing the efficiency of the proposed AFM. Furthermore, at *Point-A*, the efficiency decreases as Hr increases because the copper loss becomes markedly larger. The increase in the copper loss extremely affects the efficiency because the copper loss is dominant at this operating point.

From the above, in high-torque and low-speed regions like *Point-A*, an SMC with low permeability is not suitable for

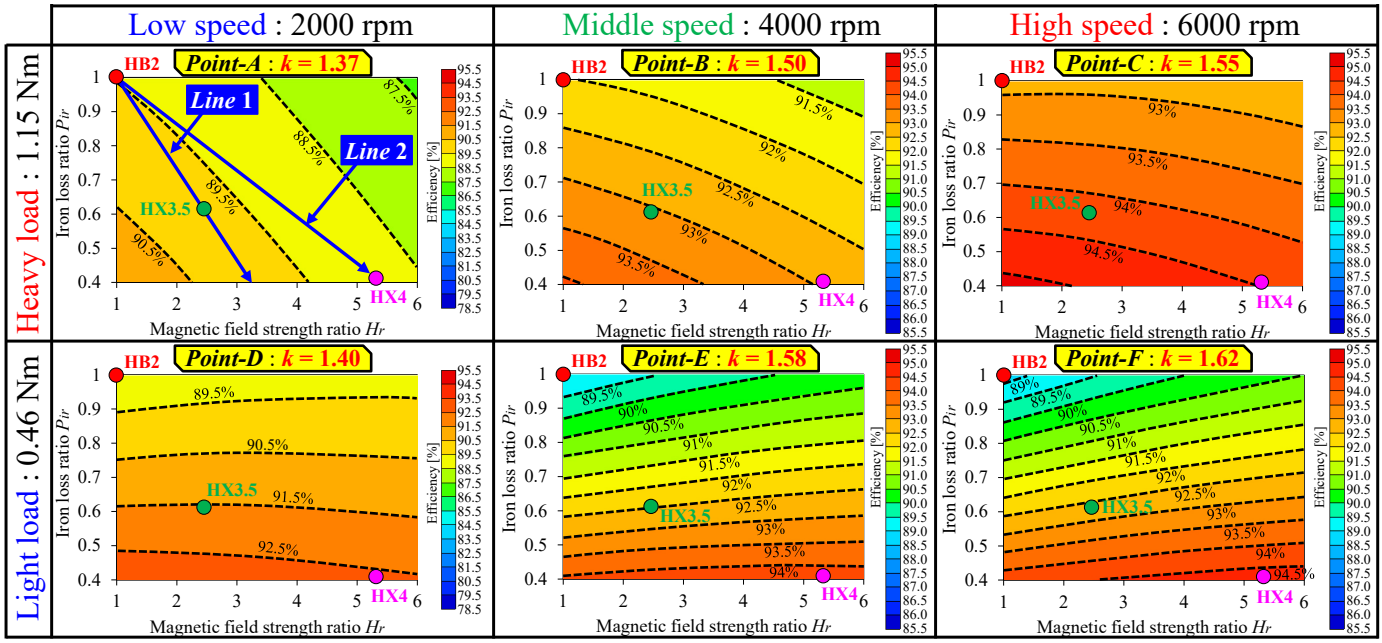

Fig. 17. Efficiency maps considering the loss ratio k in Fig. 14 at some operating points under constant average torque condition in different SMC materials (Hr = from 1 to 6, Pir = from 1.0 to 0.4).

improving efficiency. The best way to increase the efficiency at *Point-A* is to decrease *Pir* without increasing *Hr*. However, reducing the iron loss of the SMC without reducing the permeability is not easy owing to the trade-off relationship. However, if characteristics of the SMC are changed along *Line* 1 in Fig. 17 by using a slight increase in *Hr* and decrease in *Pir*, there is almost no variation in the efficiency at *Point-A*. However, when SMCs are developed along *Line* 1, the efficiency can be dramatically improved under all operating conditions apart from *Point-A*.

Second, as the rotational speed increases like at *Points-B* and *-C*, although the large copper loss is the same as at *Point-A*, the decrease in efficiency as *Hr* is increased is moderate because the proportion of the iron loss increases. In other words, the reduction in the efficiency caused by the increase in *Hr* is smaller than at *Point-A*. If the characteristics of the SMC are changed along *Line* 2 in the figure, the efficiency at *Point-A* is reduced, unlike *Line* 1. Although the slope of *Line* 2 is lower than that of *Line* 1, in case where an SMC is developed along *Line* 2, the efficiency can be dramatically improved under all operating conditions apart from *Point-A,* the same as for *Line* 1. For instance, if a newly developed SMC (HX4) that is on *Line* 2 is employed, the efficiency at *Points-C* and *-F* can be increased by 2 percentage points and 5.5 percentage points even though *Hr* is five times that of HB2. This means that the efficiency can be dramatically improved by SMCs having low permeability, especially at high speeds. This is very useful in industrial applications where high rotational speed is required.

The same tendency as *Points-A*, *-B*, and *-C* is also obtained in the light load (0.46 Nm) region. At light load *Points-D*, *-E*, and *-F*, the copper loss, which accounted for most of total loss at the heavy load (1.15 Nm) operating points, is reduced, and the iron loss thus has a greater effect on the efficiency than in the heavy load region. At light load *Points-D*, *-E*, and *-F*, the efficiency can be obviously improved by increasing *Hr* even if *Pir* remains 1.0, because the amount of decrease in the iron loss is larger than the amount of increase in the copper loss. At *Point-F* in particular, if *Hr* is changed from 1 to 6 without changing *Pir*, the efficiency of the proposed AFM can be increased by approximately 1.5 percentage point, as shown in Fig. 17.

Accordingly, in the low-torque region, which is dominated by iron loss, the efficiency can be improved by only decreasing the permeability of the SMC without reducing the iron loss. Moreover, since the iron loss is dominant in the low-torque region, the effect of reducing the iron loss of the SMC is extremely large. Consequently, the efficiency can be dramatically improved by increasing *Hr* and decreasing *Pir* at the same time in the low-torque region.

V. Experiments of Prototypes Employing Newly Developed SMC Materials (HX3.5, HX4)

A. Characteristics of newly developed SMCs

In a laboratory of Sumitomo Electric Industries, Ltd., two SMC materials (HX3.5 and HX4) are newly developed by following the development guidelines proposed in this paper. Fig. 18 shows a photograph of three manufactured stators employing HB2, HX3.5, and HX4 for the stator core. All stators have the same parameters apart from the SMC material. In addition, since the proposed AFM employs the double-stator single-rotor structure, each prototype has two identical stators, as shown in Fig. 18.

Fig. 19 shows the measured *B-H* characteristics of conventional HB2 and newly developed HX3.5 and HX4. A general laminated steel sheet (35A360) is also included in Fig. 19 as an example for better comparison. Fig. 19(a) shows the overall *B-H* characteristics of the SMCs. HB2 has the highest magnetic flux density among the three SMCs, and HX3.5 and

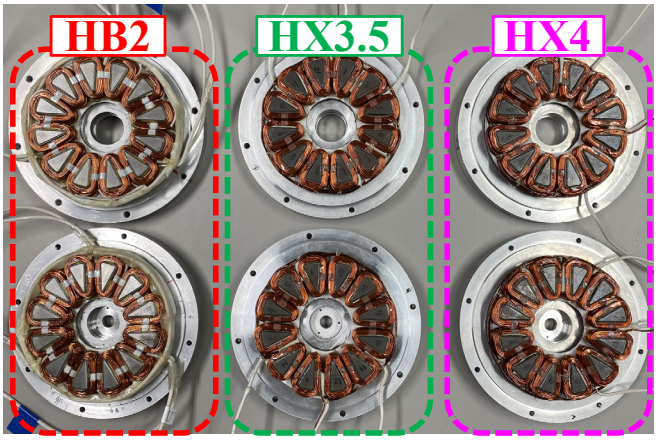

Fig. 18. Manufactured stators using HB2 and two newly developed SMCs (HX3.5, HX4).

HX4 have lower magnetic flux density than HB2, that is, lower permeability. Fig. 19(b) shows the linear region of the same *B-H* curves. The magnetic field strength ratio *Hr* is evaluated at 0.7 T in each material in Fig. 19(b). Therefore, it is obvious that the two newly developed SMCs have larger *Hr* than HB2. Although the laminated steel sheet 35A360 has higher permeability than that of the three SMCs, it is not very effective in enhancing the torque in the proposed AFM because it employs a coreless rotor structure and wide air gap.

Fig. 20 show the iron loss density of the three SMCs and laminated steel sheet. HB2 obviously has good iron loss properties because its iron loss density is lower than that of 35A360 over 400 Hz. In addition, HB2 has almost the same iron loss as 35A360 under 400 Hz. HX3.5 and HX4 have much lower iron loss compared with HB2, with the iron loss of HX4 in particular is approximately 60% lower than that of HB2.

From Figs. 19 and 20, it can be seen that three SMCs have a trade-off relationship between iron loss and permeability, as previously discussed. This means that HX3.5 and HX4 sacrifice permeability in order to reduce iron loss. However, based on the investigation in Section IV, it is predicted that the efficiency of the proposed AFM can be dramatically improved by employing the newly developed SMCs.

Table II lists *Hr* and *Pir* of the three SMCs evaluated from Figs. 19 and 20. Fig. 21 shows a comparison of the characteristics of the three SMCs on the same map as in Fig. 17. *Lines* 1 and 2 described in Section IV are also included in Fig. 21. HX3.5 and HX4 are on *Lines* 1 and 2, respectively. HX3.5 has parameters of *Hr* = 2.45, *Pir* = 0.61, and therefore, the permeability is over 50% lower than that of HB2. HX3.5 also has a 39% lower iron loss than HB2. HX4 has parameters of *Hr* = 5.33, *Pir* = 0.41. Accordingly, the permeability is over 80% lower than that of HB2, and the iron loss is also 59% lower. In addition, *Hr* and *Pir* of the laminated steel sheet 35A360 are 0.14 and 1.71, respectively.

HX3.5 has a higher reduction ratio of iron loss against decrease in permeability compared with HX4 because the slope of *Line* 1 is larger than that of *Line* 2 in Fig. 21. However, it is difficult to further reduce the iron loss of HX3.5, and in order to achieve even lower iron loss, it is necessary to further reduce

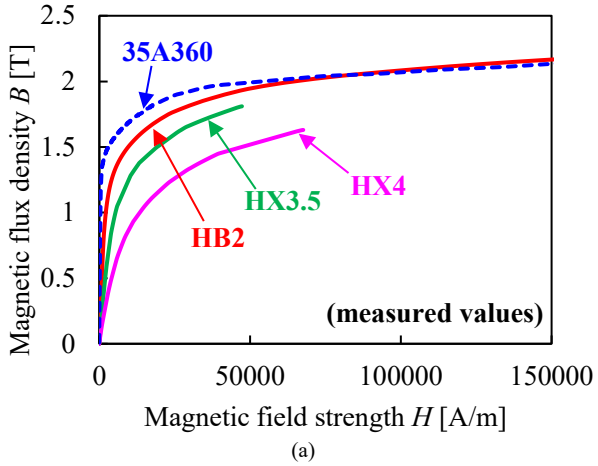

(a)

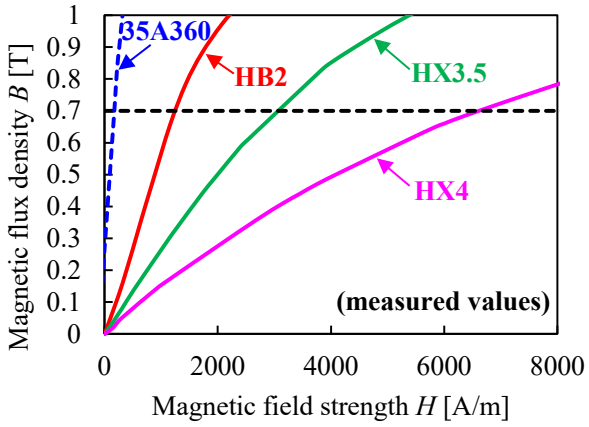

(b)

Fig. 19. Measured *B-H* characteristics of the three developed SMC materials. (a) Overall characteristics including saturated region. (b) Linear region.

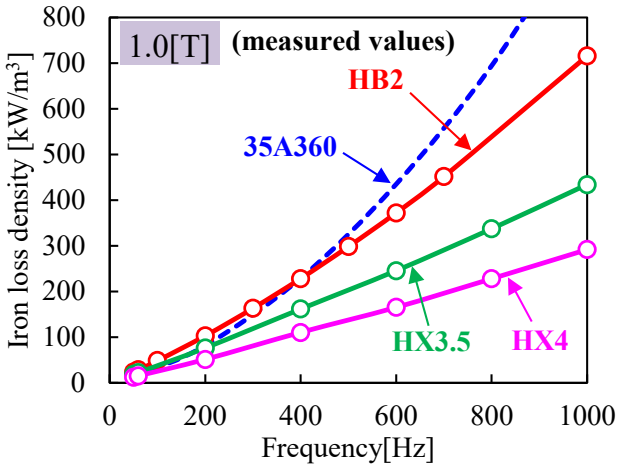

Fig. 20. Measured iron loss density of the three developed SMC materials.

the permeability as with HX4 on *Line* 2.

In addition, mechanical properties of the newly developed SMCs are different from the conventional material. However, they have enough mechanical properties from the perspective of the manufacturing process because the stator core of the three prototypes shown in Fig. 18 are manufactured by press-forming.

B. Test results of the prototype using HX3.5 and HX4

Experiments were performed under various load conditions

on prototypes employing the newly developed HX3.5 and HX4. The stator is shown in Fig. 18, and the rotor is the same as the HB2 prototype shown in Fig. 2. The system shown in Fig. 11 is used as the test platform. The maximum rotational speed and the rated current density are respectively set to 6000 rpm and 4.0 Arms/mm^2 in all prototypes, as shown in Table III. In addition, the switching frequency of the inverter is 10 kHz, and the ambient temperature of the experimental laboratory is 20 °C.

Fig. 22 shows a comparison of the average torque between measured and 3D-FEA predicted values at 1000 rpm and 4.0 Arms/mm^2. The solid line shows the measured average torque of the three prototypes with different SMCs. The dashed line shows 3D-FEA predicted values obtained by using virtual SMCs with different *Hr*. The measured values are in good agreement with the 3D-FEA values, and the reduction in the average torque is also minimized by the coreless rotor structure and the wide air gap in the experiments.

Fig. 23 shows the efficiency maps in experiments of the proposed AFM employing HX3.5 and HX4. Both prototypes achieve higher efficiency than the prototype using HB2 under almost all operating conditions. The highest efficiency of the prototype using HX3.5 and HX4 is higher than that of HB2. In the case of HB2, the highest efficiency is 92.9% at 6000 rpm, 1.2 Nm, as shown in Fig. 13(b). In the case of HX3.5, the highest efficiency is 94.4% at 6000 rpm, 1.05 Nm. Furthermore, the proposed AFM using HX4 achieved an extremely high efficiency of over 96% at 6000 rpm, 0.8 Nm in the experiment.

As described in Fig. 22, the average torque is reduced by the larger *Hr* of HX3.5 and HX4 compared to HB2. As a result, the lines in Fig. 23 representing 4.0 Arms/mm^2 are shifted toward the low torque direction.

Fig. 24 shows the difference in efficiency between HB2 (Fig. 13(b)) and the newly developed SMCs. In the experiments, the accuracy of the measured values at low torques of under 0.4 Nm and low speeds of under 2000 rpm is not high. Hence, the above area is removed from Fig. 24.

Fig. 24(a) shows the difference in the efficiency between HB2 and HX3.5. The proposed AFM using HX3.5 achieves a higher efficiency than does HB2 under all operating conditions as mentioned above. In particular, the difference in efficiency increases as the torque decreases. This is because iron loss dominates in the low-torque region. Accordingly, the difference at *Points-D*, *-E*, and *-F* is larger than that at *Points-A*, *-B*, and *-C*. In addition, the difference at *Point-F* is the largest in the low-torque region (*Points-D*, *-E*, and *-F*) since the iron loss ratio increases with increasing rotational speed. As a result, the difference in the efficiency at *Point-F* is the largest among the 6 operating points, at approximately +4.6 percentage points.

Fig. 24(b) shows the difference in the efficiency between HB2 and HX4. The overall tendency in the map is the same as for Fig. 24(a). Accordingly, the difference in the efficiency at *Point F* is the largest among the 6 operating points. In the prototype using HX4, the increase in the efficiency is larger than that of HX3.5 in almost all areas. The reasons are follows:

1) The iron loss is dominant in almost all of the areas (Fig. 16) in the proposed AFM;

TABLE II. VALUES OF *Hr* AND *Pir* OF THREE SMC MATERIALS.

Materials	Parameters	
	Hr	*Pir*
HB2	1.00	1.00
HX3.5	2.45	0.61
HX4	5.33	0.41

TABLE III. CONDITIONS OF EXPERIMENTS.

Parameters	Values
Maximum rotational speed	6000 rpm
Rated current density	4.0 Arms/mm^2
DC-bus voltage	200 V
Switching frequency *fsw*	10 kHz
Ambient temperature	20 deg. C

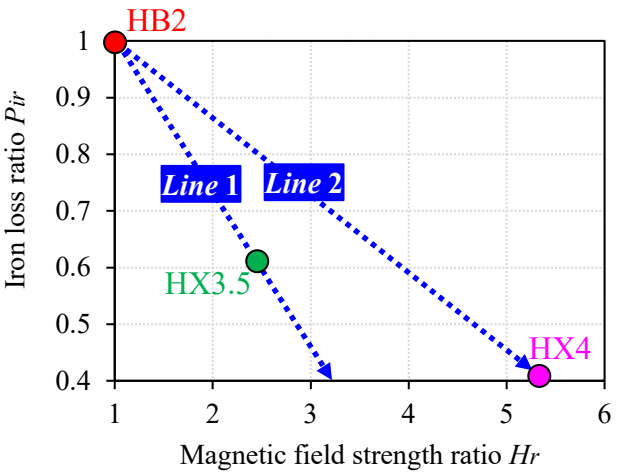

Fig. 21. Comparison of *Hr* and *Pir* of three SMC materials on the map with the *Line* 1 and the *Line*2.

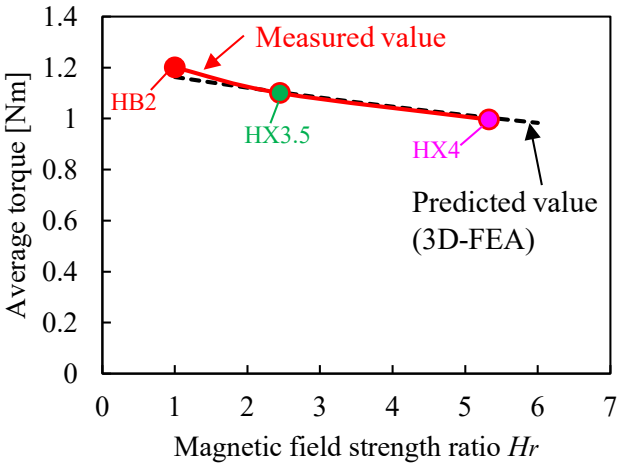

Fig. 22. Comparison of the average torque between measured and 3D-FEA predicted values (@1000 rpm, 4.0 Arms/mm^2).

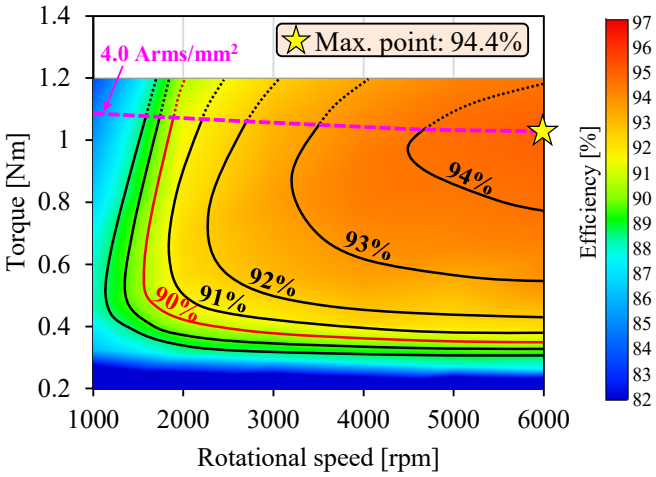

(a)

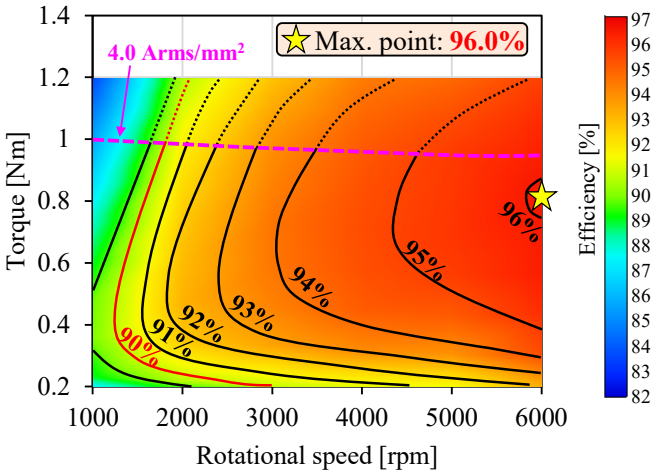

(b)

Fig. 23. Efficiency maps in experiments of the proposed AFM using newly developed SMC materials. (a) HX3.5. (b) HX4.

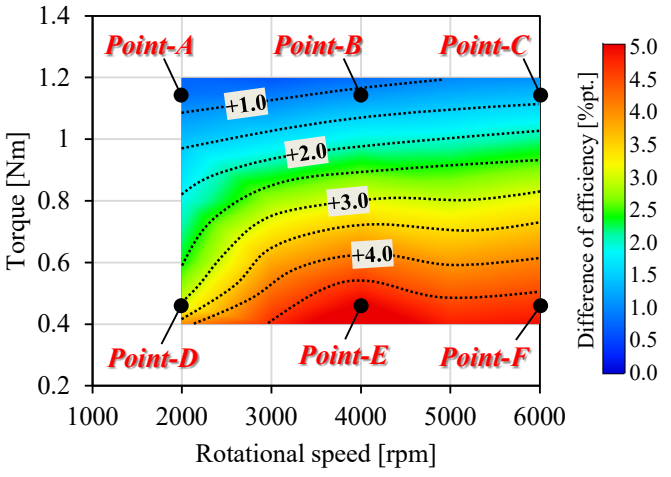

(a)

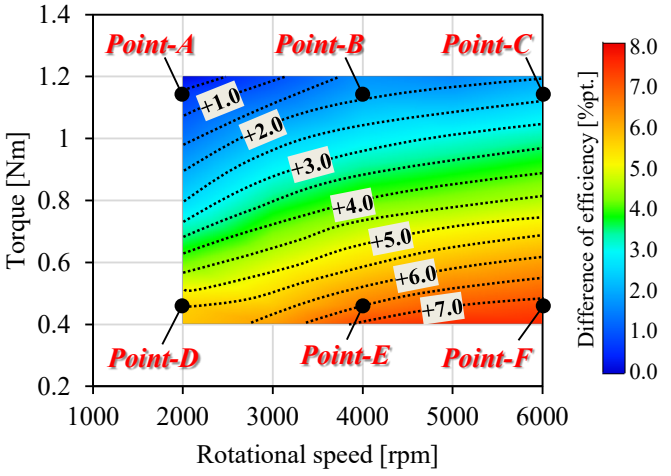

(b)

Fig. 24. Difference of efficiency between HB2 and newly developed SCMs in the proposed AFM. (a) HX3.5 - HB2. (b) HX4 - HB2.

2) The decrease in the efficiency caused by large *Hr* is limited by the coreless rotor structure;
3) HX4 can be developed with lower iron loss than can HX3.5 by sacrificing the permeability.

Consequently, the proposed AFM employing HX4 can achieve a high efficiency of over 90.0% under almost all operating conditions, and had the highest efficiency of 96.0% among the three prototypes.

C. Comparison between experiments and 3D-FEA values

It is important to evaluate the relationship between 3D-FEA predicted values using virtual SMCs considering the total loss ratio *k* and the experimental results of the prototype employing newly developed SMCs. Fig. 25 shows a comparison of the 3D-FEA predicted and measured efficiencies of the prototypes at the 6 operating points. The 3D-FEA predicted values considering the total loss ratio *k* can be confirmed in Fig. 17, and the characteristics of HX3.5 and HX4 are also plotted in Fig. 17 for ease of understanding. In Fig. 25, 3D-FEA predicted and measured values of the efficiency are shown by hatched and filled patterns, respectively.

First, in terms of HX3.5, 3D-FEA predicted values at all points are improved compared with HB2, as mentioned in Section IV. As a result, the measured values at all points also exceed the values of HB2. In addition, 3D-FEA predicted values are in good agreement with measured values at all points. This is because the total loss ratio *k* is considered in 3D-FEA.

For HX4, 3D-FEA predicted values at all points are improved compared with HB2 apart from *Point-A*. At *Point-A*, the copper loss is dominant, so that the efficiency is strongly affected by the large *Hr* of HX4. However, the measured value at *Point A* exceeds the value of HB2 unlike the 3D-FEA predicted value. The reason is that the total loss ratio *k* is different between HB2 and HX4. The 3D-FEA predicted values in Fig. 25 are evaluated by *k* that is calculated from the results for HB2. However, the total loss ratio *k* in HX4 is lower than in HB2. In other words, the increase in the iron loss of HX4 in experiments is smaller than in HB2 because the original iron loss is low. Consequently, the AFM prototype using HX4 achieves slightly higher efficiency than the 3D-FEA predicted values of HX4 at all points. This means that higher efficiency might be basically achieved than the predicted values by using the SMC development guidelines proposed in this paper. Ultimately, the AFM using HX4 exhibits higher efficiency than the HB2 at all operating points in the experiments.

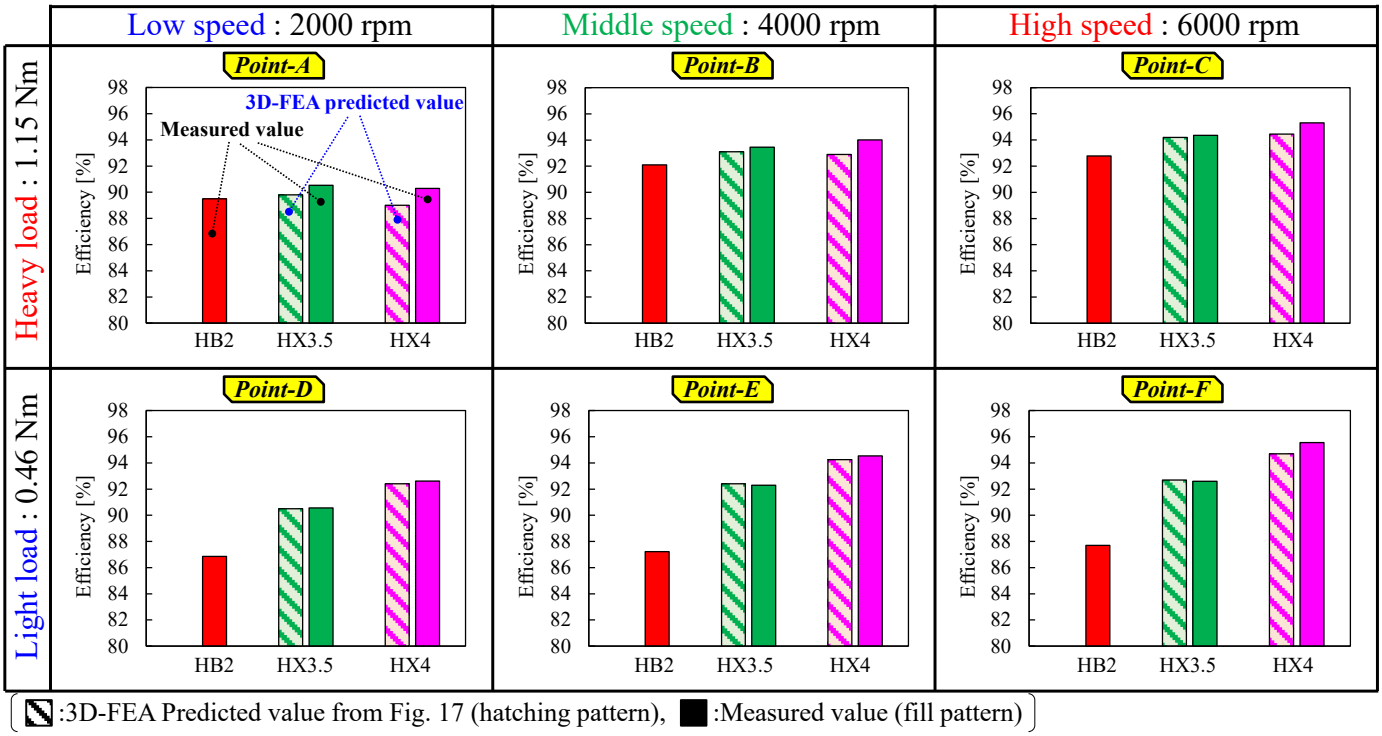

Fig. 25. Comparison of 3D-FEA predicted and measured efficiency of three prototypes using different SMC materials at 6 operating points.

VI. Development Policy of the SMC

Section IV described effectiveness of predicting the efficiency by using virtual SMCs. In Section V, validation of the prototypes using newly developed SMCs was carried out. In this section, the development guideline of the SMC is described by using some case studies including *Lines* 1 and 2 as examples.

Fig. 26 shows *Lines* 1 and 2 expressed as mathematical formulas. Since materials are generally developed based on the iron loss, the horizontal axis shows the iron loss ratio *Pir* unlike the previous figures. In other words, *Hr* is expressed as a function of *Pir*. In cases where the efficiency is enhanced by decreasing the iron loss like for *Lines* 1and 2, it is necessary to clarify the extent to which the decrease in the permeability of the SMC with decreasing *Pir* can be tolerated like Fig. 26.

For example, if a developer wants to achieve *Pir* = 0.7 on *Line* 1, *Hr* is calculated as 2.12 based on the mathematical formulas in Fig. 26. Accordingly, approximately 50% lower permeability is permitted in a newly developed SMC material. In addition, a developer can evaluate the increase in the efficiency against the original value (here, HB2) by Fig. 27. Moreover, in developing the SMC along *Line* 2 including HX4, the tolerance level of the increase in *Hr* on *Line* 2 is larger than that on *Line* 1. If a new SMC is developed in *Regions-I* or *-II* shown in Fig. 26, the efficiency can be improved at almost all operating points, as mentioned in Section V. However, in *Region-II* between *Lines* 1 and 2, the efficiency at *Point A* might not be improved very much. Developing SMCs in *Region-I* is highly difficult because the tolerance of *Hr* is smaller than at *Line* 1. Therefore, it is important to decide the development line of the SMC like *Line* 1 or *Line* 2 depending on target operating

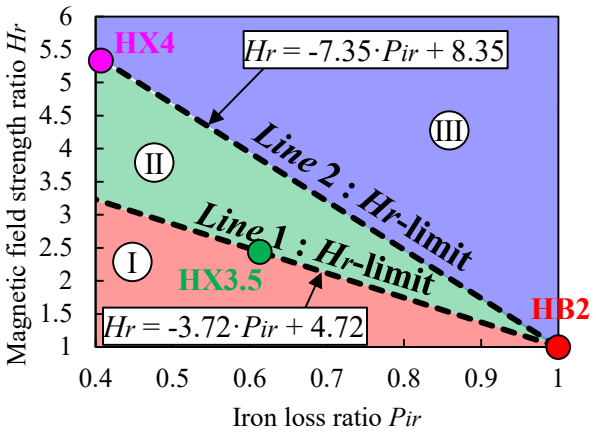

Fig. 26. *Hr*-limit-lines when new SMCs are developed along *Line*1 and *Line*2.

points of the AFM. Furthermore, if it is desired to improve the efficiency in the medium and light load regions while ignoring the reduced efficiency in the heavy load region, it is possible to consider SMCs having the characteristics in *Region-III* in Fig. 26.

Fig. 27 shows the variation in the difference in efficiency between HB2 and the virtual SMCs considered along *Lines* 1 or 2 at the 6 operating points. In Fig. 27(a), which shows the case for *Line* 1, the increase in the efficiency is small at *Point-A*. However, if *Pir* is reduced and *Hr* is increased along *Line* 1, the efficiency at almost all operating points becomes higher than the case of HB2. In particular, the effect on the efficiency at operating points where the iron loss is dominant like *Points-D*, *-E*, and *-F* is much larger compared with other points. In the case of *Pir* = 0.4, the efficiency at *Point-F* is approximately 5.8 percentage points higher than HB2.

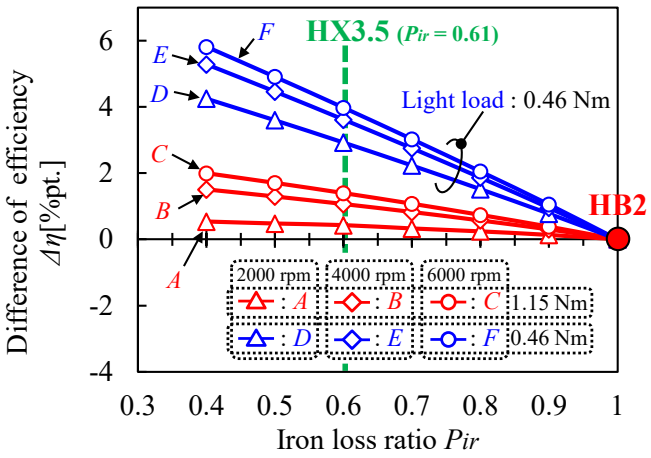

(a)

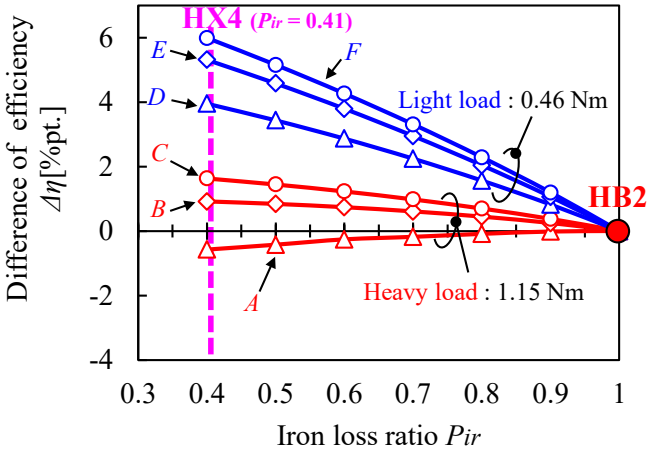

(b)

Fig. 27. Change in the difference of efficiency against existing material HB2 in case that virtual SMC materials are selected along *Line*1 and *Line*2. (a) *Line* 1: $Hr = -3.72 \cdot Pir + 4.72$. (b) *Line* 2: $Hr = -7.35 \cdot Pir + 8.35$.

In Fig. 27(b) which shows the case for *Line* 2, if *Pir* is reduced and *Hr* is increased along *Line* 2, the efficiency at all operating points apart from *Point-A* becomes higher than the case of HB2. The reason that the efficiency at *Point-A* decreases is that the copper loss becomes more dominant than the iron loss. However, in experiments, the efficiency at *Point-A* might be higher than HB2 because the total loss ratio *k* is different from HB2 as shown by experimental results of HX4. In addition, the characteristics of HX3.5 and HX4 are added to Fig. 27. In the case of HX4, *Pir* is lower than HX3.5 although *Hr* is larger, and as a result, the overall efficiency of the AFM increases as shown in Fig. 27.

From the above, the analytical and experimental results show that the efficiency of the proposed AFM using the coreless rotor structure can be dramatically improved by changing the permeability and iron loss of the SMC.

VII. Conclusion

This paper proposed SMC development guidelines suitable for improving the efficiency of AFMs. In general, SMCs have a trade-off relationship between iron loss and magnetic permeability. However, the proposed AFM can avoid reduction in average torque caused by low permeability of the SMC because it uses a coreless rotor structure and wide air gap. The efficiency of the proposed AFM can then be improved by

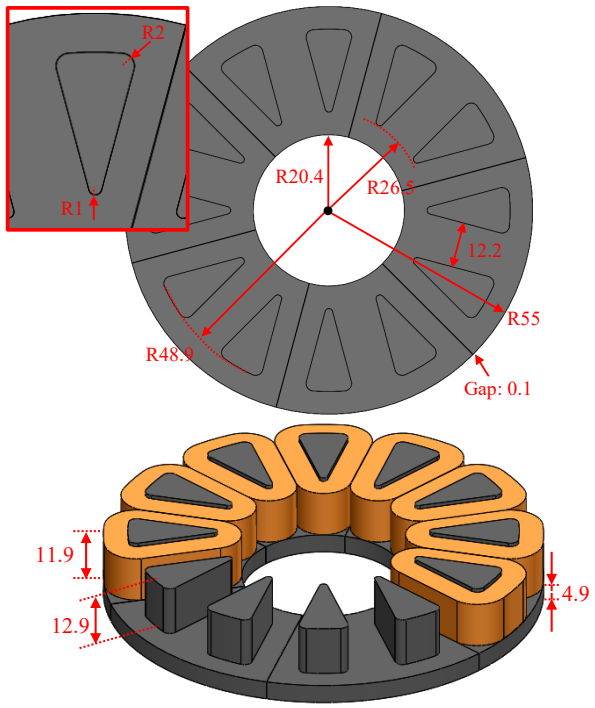

Fig. 28. Stator model and dimensions of the investigated AFM in this paper.

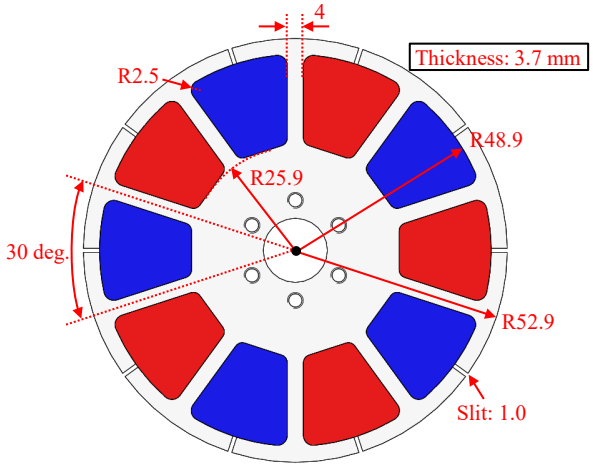

Fig. 29. Rotor model and dimensions of the investigated AFM in this paper.

TABLE IV. Basic Parameters of The Investigated AFM

Parameters	Value
Axial length *L* (assembly)	41.3 mm
Outer diameter *D* (assembly)	110 mm
The number of poles / slots	10 poles / 12 slots
Air gap length	1.0 mm
Coil space factor	40%
The number of turns	46 turn/slot
Total weight of magnet	89.2 g
Rated current density	4.0 Arms/mm^2
DC-bus voltage	200 V
Maximum rotational speed	6000 rpm

reducing the iron loss of the SMC without large reduction of the torque.

In addition, this paper constructed SMC development guidelines based on experimental results, and therefore the accuracy of the 3D-FEA predicted efficiency is high. Furthermore, in a laboratory of Sumitomo Electric Industries, Ltd., two new SMC materials (HX3.5, HX4) were developed based on the development guidelines proposed in this paper. The proposed AFM employing HX4 in particular achieves a high efficiency of over 90.0% over a wide operating range, and the highest efficiency is over 96.0% in experiments. The efficiency of AFMs is able to be dramatically improved by using the proposed development guidelines. In the final section, the SMC development guidelines are described in detail by using some case studies including *Lines* 1 and 2. Developers in many research groups can design new SMC materials suitable for each AFM based on this paper.

APPENDIX

Figs. 28 and 29 show detailed parameters and dimensions of the proposed AFM investigated in this paper. Table IV lists basic parameters such as operating conditions and winding. In this paper, 3D-FEA is executed by using an electromagnetic field simulator (JMAG-designer ver. 20.0, JSOL Co., Ltd.). In addition, the above simulator includes HB2, which as an existing SMC material.

ACKNOWLEDGMENTS

This work was supported by the Japan Society for the Promotion of Science (JSPS) KAKENHI Grant No. 20J10951.

REFERENCES

[1] A. De Almeida, F. Ferrieira, and G. Baoming, “Beyond Induction Motors - Technology Trends to Move Up Efficiency,” *IEEE Trans. Industry Applications*, vol. 50, no. 3, pp. 2103-2114, May/June 2014.

[2] A. De Almeida, F. Ferreira, J. Fong, and P. Fonseca, “EuP Lot 11 Motors, Ecodesign Assessment of Energy Using Products,” *ISR-Univ. Coimbra,Brussels, Belgium, Final Report for the European Commission,* Feb. 2008.

[3] R. Tsunata, M. Takemoto, S. Ogasawara, A. Watanabe, T. Ueno, and K. Yamada, “Development and Evaluation of an Axial Gap Motor Using Neodymium Bonded Magnet,” *IEEE Trans. Industry Applications*, vol. 54, no. 1, pp. 254-262, Jan./Feb. 2018.

[4] D. Winterbourne, N. Stannard, L. Sjoberg, and G. Atkinson, “An Air-Cooled YASA Motor for in-Wheel Electric Vehicle Applications,” *IEEE Trans. Industry Applications*, vol. 56, no. 6, pp. 6448-6455, Nov./Dec. 2020.

[5] S. Mirimani, A. Vahedi, F. Marignetti, and E. De Santis, “Static Eccentricity Fault Detection in Single-Stator-Single-Rotor Axial-Flux Permanent-Magnet Machines,” *IEEE Trans. Industry Applications*, vol. 48, no. 6, pp. 1838-1844, Nov./Dec. 2012.

[6] G. D. Donato, F. G. Capponi, G. A. Rivellini, and F. Caricchi, “Integral-Slot Versus Fractional-Slot Concentrated-Winding Axial-Flux Permanent-Magnet Machines: Comparative Design, FEA, and Experimental Tests”, *IEEE Transactions on Industry Application*, vol. 48, No. 5, Sep./Oct. 2012, pp. 1487-1495.

[7] Y. Li, Z. Q. Zhu, G. J. Li, “Influence of Stator Topologies on Average Torque and Torque Ripple of Fractional-Slot SPM Machines With Fully Closed Slots”, *IEEE Transactions on Industry Application*, vol. 54, No. 3, May/June 2018, pp. 2151-2164.

[8] R. Tsunata, M. Takemoto, S. Ogasawara, A. Watanabe, T. Ueno, and K. Yamada, “Investigation of Enhancing Efficiency and Acceleration in a Flat Shape Axial Gap Motor Having High Torque Characteristic”, *in Proc. of the 2017 IEEE International Conference on Mechatronics (ICM2017)*, 2017, Australia, 6 pages.

[9] A. Chen, R. Nilssen, and A. Nysveen, “Performance Comparison Among Radial-Flux, Multistage Axial-Flux, and Three-Phase Transverse-Flux PM Machines for Downhole Applications,” *IEEE Trans. Industry Applications*, vol. 46, no. 2, pp. 779-789, March/April. 2010.

[10] F. Marignetti, V. D. Colli, and S. Carbone, “Comparison of Axial Flux PM Synchronous Machines With Different Rotor Back Cores,” *IEEE Trans. Magnetics*, vol. 46, no. 2, pp. 598-601, Feb. 2010.

[11] H. Qiu, W. Yu, B. Tang, Y. Mu, W. Li, and C. Yang, “Study on the Influence of Different Rotor Structure on the Axial-Radial Flux Type Synchronous Machine,” *IEEE Trans. Industrial Electronics*, vol. 65, no. 7, pp. 5406-5412, July 2018.

[12] F. Profumo, Z. Zhang, and A. Tenconi, “Axial Flux Machines Drives: A New Viable Solution for Electric Cars,” *IEEE Trans. Industrial Electronics*, vol. 44, no. 1, pp. 39-44, Feb. 1997.

[13] Z. Frank, and J, Laksar, “Analytical Design of Coreless Axial-Flux Permanent Magnet Machine With Planar Coils,” *IEEE Trans. Energy Conversion*, vol. 36, no. 3, pp. 2348-2357, Sept. 2021.

[14] N. Taran, V. Rallabandi, G. Heins, and D. M. Ionel, “Coreless and Conventional Axial Flux Permanent Magnet Motors for Solar Cars,” *IEEE Trans. Industry Applications*, vol. 54, no. 6, pp. 5907-5917, Nov./Dec. 2018.

[15] R. Tsunata, M. Takemoto, S. Ogasawara, T. Saito, and T. Ueno, “Development Policy of SMC to Improve Efficiency of Axial Gap Motor Employing Coreless Rotor Structure,” *in Proc. of the 2020 IEEE International Conference on Electrical Machines (ICEM2020)*, 2020, Gothernburg, Sweden, pp. 1644-1650.

[16] M. Geest, H. Polinder, and J. A. Ferreira, “Influence of PWM switching frequency on the losses in PM machines,” *in Proc. of the 2014 IEEE International Conference on Electrical Machines (ICEM2014)*, 2014, Berlin, Germany, pp. 1243-1247.

[17] A. Krings, J. Soulard, and O. Wallmark, “PWM Influence on the Iron Losses and Characteristics of a Slotless Permanent-Magnet Motor With SiFe and NiFe Stator Cores,” *IEEE Trans. Industry Applications*, vol. 51, no. 2, pp. 1475-1485, March/April 2015.

[18] R. Tsunata, M. Takemoto, S. Ogasawara, K. Orikawa, T. Saito, T. Ueno, “Examination of Enhancing Efficiency of Axial Gap Motor in High Speed and High Torque Region by Adopting Neodymium Bonded Magnet,” *IEEJ Journal of Industry Applications*, vol. 10, no. 4, pp. 487-496, 2021.

[19] D. Gumbleton-Wood, G. Atkinson, J. Washington and L. Sjöberg, “The influence of production methods on the magnetic performance of electrical steels and soft magnetic composites,” *in Proc. of the 2017 IEEE International Electric Machines and Drives Conference (IEMDC)*, 2017, Miami, FL, USA, pp. 1-7.

[20] L. Hegedűs *et al*., “Energy Losses in Composite Materials Based on Two Ferromagnets,” *IEEE Trans. Magnetics*, vol. 53, no. 12, 6 pages, Dec. 2017.

[21] Jana Füzerová *et al*., “Analysis of the Complex Permeability Versus Frequency of Soft Magnetic Composites Consisting of Iron and $Fe_{73}Cu_1Nb_3Si_{16}B_7$,” *IEEE Trans. Magnetics*, vol. 48, no. 4, 4 pages, April, 2012.

[22] Y. Shimada, T. Nishioka, and A. Ikegaya, “Development of High-Performance P/M Soft Magnetic Material”, *Journal of the Japan Soc. of Powder and Powder Metallurgy*, vol. 53, No. 8, June 2006, pp. 686-695.

[23] T. Iwasaki, M. Inamori, M. Morimoto, “Variation of iron loss by manufacturing method of SMC motor core”, *in Proc. of the 2017 IEEE International Conference on Electrical Machines and Systems (ICEMS2013)*, Busan, Korea, Oct. 26-29, 2013, pp. 2040-2043.

[24] M. Nakano, C. Fujino, Y. Tani, A. Daikoku, Y. Toide, S. Yamaguchi, H. Arita, T. Yoshioka, “High-Precision Calculation of Iron Loss by Considering Stress Distribution on Magnetic Core,” *IEEJ Journal of Industry Applications*, vol. 129, no. 11, pp. 1060-1067, 2009 (Japanese).

[25] H. Qin, H. Ni and J. Jin, “Differential Evolutionary Modeling and Starting-up Cavitation Characteristics Analysis for Multistage Centrifugal Pump,” *in Proc. of the 2018 IEEE 4th Information Technology and Mechatronics Engineering Conference (ITOEC)*, pp. 412-416, 2018.

Ren Tsunata was born in Miyagi Prefecture, Japan, in 1992. He received the B.S., M.S., and Ph.D. degrees in electrical engineering from Hokkaido University, Hokkaido, Japan, in 2015, 2017, and 2021, respectively. He was with Toyota Motor Corporation, Aichi, Japan, in 2017-2018. In 2021, he joined Okayama University as a Research Fellow. Since 2022, he has been an Assistant Professor with the Graduate School of Natural Science and Technology, Okayama University, Okayama, Japan. His research interests include permanent magnet synchronous machines, variable flux motors, and axial flux machines.

Dr. Tsunata is a member of the Institute of Electrical Engineers of Japan (IEEJ) and The Japan Society of Applied Electromagnetics and Machines (JSAEM). Dr. Tsunata was a recipient of four IEEJ Excellent Presentation Awards in 2017, 2020 and 2022, and the Incentive Award from JSAEM in 2020..

Masatsugu Takemoto (M'99) was born in Tokyo, Japan, in 1972. He received the B.S. and M.S. degrees in electrical engineering from the Tokyo University of Science, Noda, Japan, in 1997 and 1999, respectively, and the Ph.D. degree in electrical engineering from the Tokyo Institute of Technology, Tokyo, in 2005. In 1999, he joined the Tokyo Institute of Technology as a Research Associate in the Department of Electrical Engineering. In 2004, he joined the Musashi Institute of Technology, Tokyo, as a Research Associate in the Department of Mechanical Systems Engineering, where he became a Lecturer in 2005. In 2008, he joined Hokkaido University as an Associate Professor in the Graduate School of Information Science and Technology. Since 2020, he has been with Okayama University, where he is a Professor in the Graduate School of Natural Science and Technology. He is engaged in research on permanent magnet synchronous motors, axial gap motors, rare-earth-free motors, bearingless motors, and magnetic bearings.

Dr. Takemoto is a member of IEEJ. He was the recipient of the Nagamori Award from the Nagamori Foundation in 2017, the IEEJ Transaction Paper Award in 2005, the Prize Paper Awards from the Electric Machines Committee of the IEEE Industry Applications Society in 2011 and 2019, and the Prize Paper Award from the Electrical Machines Technical Committee of the IEEE Industrial Electronics Society in 2018. He has served as Secretary, Vice-Chair, and Chair of the IEEE IAS Japan chapter in 2008–2009, 2010–2011, and 2012-2013, respectively.

Satoshi Ogasawara (A'87-M'93-SM'97) was born in Kagawa, Japan, in 1958. He received B.S., M.S., and Ph.D. degrees in electrical engineering from the Nagaoka University of Technology, Niigata, Japan, in 1981, 1983, and 1990, respectively. From 1983 to 1992, he was a Research Associate at Nagaoka University of Technology. From 1992 to 2003, he was in the Department of Electrical Engineering, Okayama University. From 2003 to 2007, he was in the Department of Electrical Engineering, Utsunomiya University, Utsunomiya, Japan. Since 2007, he has been a Professor with the Graduate School of Information Science and Technology, Hokkaido University. His research interests include AC motor drive systems and static power converters. Dr. Ogasawara received the IEEE Power Electronics Society Prize Paper Award in 1999 and the IEEE Industry Applications Society Committee Prize Paper Awards in 1996, 1997, 2003, and 2010. He is a fellow of the IEEJ.

Tatsuya Saito was born in Kyoto, Japan, in 1987. He received B.S., M.S., Ph.D. degrees in material science from Tohoku University, Sendai, Japan, in 2009, 2011 and 2014, respectively. Since 2014, he has been with Sumitomo Electric Industries, Ltd., Hyogo, Japan, where he is engaged in research on soft magnetic materials and powder metallurgy.

Tomoyuki Ueno was born in Wakayama Prefecture, Japan, in 1976. He received B.S. and M.S. degrees in mechanical engineering from Kobe University, Hyogo, Japan, in 1999 and 2001, respectively, and a Dr. Eng. degree in industrial innovation science from Okayama University in 2015. Since 2001, he has been with Sumitomo Electric Industries, Ltd., where he is engaged in research on soft magnetic materials, ceramics materials, and cutting and grinding technology.

Dr. Ueno is a member of the Japan Society and Power Metallurgy (JSPM) and the Japan Society for Abrasive Technology (JSAT). He has received the JSPM Award Innovatory Research in 2009, JSAT Prize Paper Award in 2012, Prize Paper Award from the Machine Tool Engineer Foundation in 2012, and JSPM Award for Innovatory Development in 2013.